Predicting Lipid-Rich Plaque Progression in Coronary Arteries Using Multimodal Imaging and Wall Shear Stress Signatures

Arteriosclerosis, Thrombosis, and Vascular Biology

TRANSLATIONAL STUDIES

Predicting Lipid-Rich Plaque Progression in Coronary Arteries Using Multimodal Imaging and Wall Shear Stress Signatures

Giuseppe De Nisco, Eline M.J. Hartman, Elena Torta, Joost Daemen, Claudio Chiastra, Diego Gallo, Umberto Morbiducci, Jolanda J. Wentzel

BACKGROUND: Plaque composition and wall shear stress (WSS) magnitude act as well-established players in coronary plaque progression. However, WSS magnitude per se does not completely capture the mechanical stimulus to which the endothelium is subjected, since endothelial cells experience changes in the WSS spatiotemporal configuration on the luminal surface. This study explores WSS profile and lipid content signatures of plaque progression to identify novel biomarkers of coronary atherosclerosis.

METHODS: Thirty-seven patients with acute coronary syndrome underwent coronary computed tomography angiography, near-infrared spectroscopy intravascular ultrasound, and optical coherence tomography of at least 1 nonculprit vessel at baseline and 1-year follow-up. Baseline coronary artery geometries were reconstructed from intravascular ultrasound and coronary computed tomography angiography and combined with flow information to perform computational fluid dynamics simulations to assess the time-averaged WSS magnitude (TAWSS) and the variability in the contraction/expansion action exerted by WSS on the endothelium, quantifiable in terms of topological shear variation index (TSVI). Plaque progression was measured as intravascular ultrasound-derived percentage plaque atheroma volume change at 1-year follow-up. Plaque composition information was extracted from near-infrared spectroscopy and optical coherence tomography.

RESULTS: Exposure to high TSVI and low TAWSS was associated with higher plaque progression (4.00±0.69% and 3.60±0.62%, respectively). Plaque composition acted synergistically with TSVI or TAWSS, resulting in the highest plaque progression (≥5.90%) at locations where lipid-rich plaque is exposed to high TSVI or low TAWSS.

CONCLUSIONS: Luminal exposure to high TSVI, solely or combined with a lipid-rich plaque phenotype, is associated with enhanced plaque progression at 1-year follow-up. Where plaque progression occurred, low TAWSS was also observed. These findings suggest TSVI, in addition to low TAWSS, as a potential biomechanical predictor for plaque progression, showing promise for clinical translation to improve patient prognosis.

GRAPHIC ABSTRACT: A graphic abstract is available for this article.

Key Words: coronary artery disease ■ hemodynamics ■ patient-specific modeling ■ plaque, atherosclerotic ■ ultrasonography

Atherosclerosis is a lipid-driven inflammatory disease representing a leading cause of morbidity and mortality in the Western world.[1] In the last decades, it has been acknowledged that blood flow-induced frictional forces on the endothelium, evaluated in terms of wall shear stress (WSS), are involved in the onset and progression of coronary atherosclerosis. Low time-averaged WSS (TAWSS) magnitude, inducing endothelial dysfunction,[2–4] promotes lipid infiltration in the arterial wall with potential atherosclerotic plaque initiation and progression.[5] In turn, the lipid plaque content has been proven to influence local inflammation, thus stimulating

Correspondence to: Umberto Morbiducci, PhD, Department of Mechanical and Aerospace Engineering, Politecnico di Torino, Corso Duca degli Abruzzi, 24, 10129 Turin, Italy. Email umberto.morbiducci@polito.it

Supplemental Material is available at https://www.ahajournals.org/doi/suppl/10.1161/ATVBAHA.123.320337.
For Sources of Funding and Disclosures, see page 985.

Arterioscler Thromb Vasc Biol is available at www.ahajournals.org/journal/atvb

Nonstandard Abbreviations and Acronyms

CCTA	coronary computed tomography angiography
CFD	computational fluid dynamics
IVUS	intravascular ultrasound
NIRS	near-infrared spectroscopy
OCT	optical coherence tomography
OSI	oscillatory shear index
PAV	plaque atheroma volume
RRT	relative residence time
TAWSS	time-averaged wall shear stress
transWSS	transverse wall shear stress
TSVI	topological shear variation index
WSS	wall shear stress
WT	wall thickness

further disease evolution.[6] Although low WSS magnitude is known to be involved in atherosclerotic plaque development,[7,8] and recently a synergistic effect of low TAWSS and lipid plaque content on plaque growth has been proven,[9,10] WSS magnitude might only partially capture the mechanical stimulus to which the endothelial cells are subjected, thus not fully reflecting their response to flow disturbances.[11,12] Over the cardiac cycle, endothelial cells experience not only temporal changes in the WSS magnitude but also changes in the spatial configuration of the WSS vector field, which might converge or diverge along critical lines on the luminal surface, resulting in a contraction or expansion action exerted on the endothelial cells (Figure S1).[13] Such hemodynamic stimuli transmitted to the endothelium induce changes in the state of cell and cell-cell tensions that impact functional biological responses[14] up to the vessel level. In detail, endothelial cells exposed to an ostensibly physiological variability in the WSS contraction/expansion action during the cardiac cycle are expected to maintain a quiescence state, with stable intercellular junctions and force transmission to remote sites throughout the cell,[3,4,14,15] preventing, for example, lipid infiltration and ultimately atherosclerotic plaque initiation.[15] On the contrary, the luminal exposure to a marked variability in contraction/expansion action of the WSS vector field may alter the endothelial cells' mechanoresponsiveness, stimulating recurring variation in intracellular as well as intercellular tensions, and ultimately their proatherogenic susceptibility.[14,16–18] Focusing on coronary arteries, recent works revealed that the variability of the WSS contraction/expansion action along the cardiac cycle, quantified in terms of topological shear variation index (TSVI),[19,20] was instrumental in identifying mild coronary lesion site of myocardial infarction at 5-year follow-up in humans[21] and in predicting wall thickness (WT) change over time (a hallmark of atherosclerosis development) in a longitudinal study on swine models.[13]

Highlights

- Wall shear stress signatures are markers of atherosclerotic disease progression in coronary arteries.
- Endothelial exposure to high wall shear stress contraction/expansion action variability results in atherosclerotic plaque progression.
- Plaque composition acts synergistically with high topological shear variation index values and low wall shear stress magnitude to atherosclerotic plaque progression.
- Topological shear variation index significantly contributes to a deeper understanding of the hemodynamic impact on coronary atherosclerosis.

Based on these recent pieces of evidence, we aimed to study the association between WSS signatures and plaque atheroma volume (PAV) temporal changes in human coronary arteries. Integrating multimodality clinical imaging using intravascular ultrasound (IVUS), near-infrared spectroscopy (NIRS), optical coherence tomography (OCT), and invasive Doppler flow measurements with computational fluid dynamics (CFD), the synergistic effect of WSS signatures (quantified by the TSVI) and plaque phenotypes on atherosclerotic plaque evolution is investigated. The hypothesis of this study is that the variability of the contraction/expansion action exerted by the WSS on endothelial cells along the cardiac cycle[13,21] is capable to predict PAV changes over time.

METHODS

Availability of Data

The data supporting the findings of this study are available from the corresponding author upon reasonable request. Methods for WSS analysis and visualization are explained in a tutorial video showing how TSVI can be obtained from CFD-derived WSS data in the open-source Paraview environment (Video S1). Additionally, a tutorial video and Python code for computing TSVI from CFD-derived WSS data in Visualization Toolkit Polygonal format are available for download in a public repository on GitHub (https://github.com/PoliToBIOMed-Lab-Cardiovascular-Biomech/TSVI).

Patients' Inclusion

The present analysis is part of the IMPACT study (Imaging and Modeling to Investigate the Mutual Relationship of Plaque Growth and Biomechanical Parameters in Human Coronary Arteries), a prospective, multimodal imaging single-center study designed with the specific goal of elucidating the role of local hemodynamics in the natural history of atherosclerosis.[9,22] To reach this goal, the IMPACT study enrolled 53 hemodynamically stable patients with an acute coronary syndrome presenting with (at least) 1 nonstented, nonculprit coronary artery accessible to Doppler guidewire and intracoronary imaging.

The presence of previous coronary artery bypass graft surgery, 3-vessel disease, renal insufficiency (creatinine clearing <50 mL/min), left ventricular ejection fraction <30%, and atrial fibrillation were considered as exclusion criteria. All patients gave their written informed consent. The study protocol was approved by the Erasmus MC local medical ethics committee (MED2015-535, NL54519.078.15) and registered (ISCRTN: 43170100). The study was conducted in accordance with the World Medical Association Declaration of Helsinki (64th WMA General Assembly, Fortaleza, Brazil, October 2013) and Medical Research Involving Human Subjects Act.

Medical Imaging

A schematic overview of the applied technologies and methodologies is reported in Figure 1. All patients underwent percutaneous coronary intervention of the culprit coronary vessel at baseline (T1). After successful treatment, a nonculprit coronary segment with at least 30 mm of length and 2 readily identifiable side branches (diameter >1.5 mm) was selected for the study. A dual-sensor NIRS–IVUS catheter (TVC [True Vessel Characterization] Insight Coronary Imaging Catheter, InfraRedX, Burlington, MA) was used for the simultaneous assessment of lipids and plaque volume. Automated motorized pullbacks were performed at 0.5 mm/s.[22] Subsequently, OCT imaging was performed within the same coronary segment of interest using the Dragonfly Optis Imaging Catheter (Abbott Vascular, Santa Clara, CA) adopting an automated pullback of 36 mm/s. To assess coronary flow distribution, local blood velocity measurements were invasively performed using a Doppler ComboWire (Phillips Volcano, Zaventem, Belgium) at different locations along the study segment (ie, proximal, and distal to each side branch). Finally, 1 month after the invasive procedure, patients underwent coronary computed tomography angiography (CCTA, SOMATOM Force; Siemens Healthineers, Germany) according to a standard prospectively ECG-triggered clinical protocol. The same invasive imaging protocol including IVUS imaging was applied at 1-year follow-up (T2). Data were anonymized and analyzed offline.

Plaque Growth and Composition

Lumen and external elastic membrane contours were semiautomatically segmented on IVUS image frames at time points T1 and T2, as reported previously.[9,23] On IVUS images, WT was measured as the radial distance between inner and outer

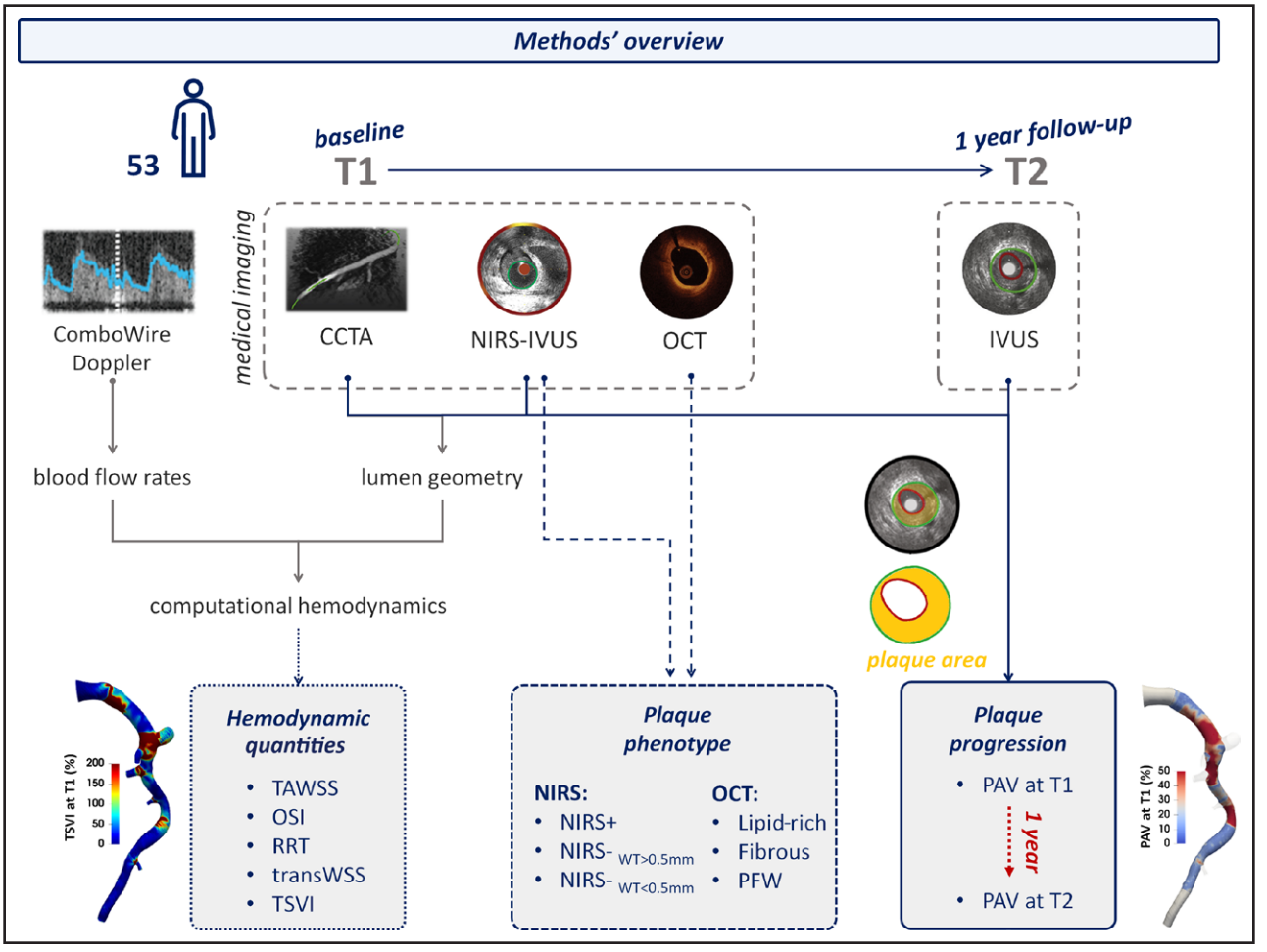

Figure 1. Schematic diagram of the study design, showing how imaging data contribute to define vessel geometry, wall shear stress–based quantities, plaque phenotype, and plaque progression.
CCTA indicates coronary computed tomography angiography; IVUS, intravascular ultrasound; NIRS, near-infrared spectroscopy; OCT, optical coherence tomography; OSI, oscillatory shear index; PAV, plaque atheroma volume; PFW, plaque-free wall; RRT, relative residence time; TAWSS, time-averaged wall shear stress; transWSS, transverse wall shear stress; and TSVI, topological shear variation index.

arterial wall contours, while percentage plaque atheroma volume was assessed in terms of the ratio between the plaque area volume and total vessel area volume, expressed as percentage value. Plaque progression was quantified as the difference between PAV values at T2 and T1 and referred as ΔPAV.

NIRS and OCT data were used to analyze plaque composition at baseline. Briefly, based on the acquired NIRS signal, an NIRS-positive classification was assigned to locations where the signal had a high probability (>0.6) for the presence of lipids, while NIRS-negative classification was attributed elsewhere. Based on OCT acquisitions, (1) locations with inhomogeneous, attenuated OCT signal with no visible external elastic membrane were classified as lipid-rich plaque; (2) locations where a lipid pool was identified as an overlying signal-rich cap structure with a sudden attenuation were classified as fibrous cap atheroma; (3) locations presenting a relatively homogeneous OCT signal with identifiable external elastic membrane were classified as fibrous plaque; (4) plaque-free wall was defined as a healthy wall with an OCT-visible 3-layered structure. Extensive details on OCT-based classification have been reported in previous studies.[9,24]

Computational Hemodynamics

The 3-dimensional geometry of coronary arteries imaged at T1 was reconstructed by fusing CCTA and IVUS images (Figure 1). In detail, the 3-dimensional model in the IVUS-imaged region was reconstructed using the spatial information extracted from CCTA, the 3-dimensional vessels centerline, to align the IVUS-based segmented lumen contours as reported in previous studies.[24,25] To do that, the MeVisLab (MeVis Medical Solutions AG, Bremen, Germany) software was used. Luminal regions proximal and distal to the imaged IVUS vessel segment were reconstructed using the lumen segmentation from CCTA images.[24,25] On the CCTA-IVUS reconstructed vessel geometries, transient CFD simulations were performed to quantify near-wall hemodynamic features, according to a previously described methodology.[26–28] In brief, the reconstructed 3-dimensional geometries were meshed, and the finite volume method was used to numerically solve the governing equations of fluid motion, the Navier-Stokes equations, in their discretized form. Blood was assumed as an incompressible, homogeneous, non-Newtonian fluid, with density of 1060 kg/m^3 and viscosity described through the Carreau fluid model.[29] The arterial walls were assumed to be rigid, and the no-slip condition was applied to them. Patient-specific boundary conditions were derived from individual in vivo intravascular Doppler velocity measurements. In detail, the inflow boundary condition was derived from the most proximal Doppler measurement as proposed elsewhere.[30] As for the conditions at outflow boundaries, the instantaneous flow ratio, evaluated from in vivo measurements as the difference between upstream and downstream Doppler measurements at each side branch, was prescribed. In case of inaccurate or unavailable Doppler velocity measurements, a generalized flow rate[31] was prescribed as inflow boundary condition, while a proper diameter-based scaling law was applied to estimate the flow ratio at the outflow sections.[9,24]

WSS-Based Quantities

Three WSS-based quantities, namely TAWSS, oscillatory shear index (OSI),[32] and relative residence time (RRT),[33] were computed. In detail, TAWSS represents the local WSS vector magnitude value averaged over the cardiac cycle; OSI quantifies the changes in direction of WSS vector during the cardiac cycle, ranging between 0 (unidirectional WSS vector) and 0.5 (purely oscillatory WSS vector); RRT is a combination of TAWSS and OSI identifying luminal regions exposed to low magnitude and highly oscillatory WSS vector. Additionally, the transverse WSS (transWSS) was considered.[34] The transWSS represents the average value over the cardiac cycle of WSS component acting orthogonal to the cycle-average WSS vector direction, and it is instrumental in quantifying the multidirectional character of WSS vector over the cardiac cycle.

The TSVI was used to measure the variability of the local contraction/expansion action exerted on the endothelium by the WSS along the cardiac cycle (as explained in Figure S1).[13,19,20]

The mathematical formulation of the hemodynamic quantities considered for the analysis is reported in Table S1.

Statistical Analysis

The coronary segments that were imaged by IVUS were used for the statistical analysis. As detailed elsewhere,[9,23,24,27] the luminal surface of the region of interest was divided into 1.5 mm/45° luminal sectors, over which continuous data (ie, WT, PAV, and WSS-based quantities) were averaged (Figure 2). Data were presented as median (interquartile range). The sector-averaged WSS-based quantities were then divided into vessel-specific tertiles (low, mid, and high). NIRS-based data were divided into 3 sector groups: NIRS-positive sectors (>50% of the sector was NIRS positive), NIRS-negative plaque sectors (>50% of the sector was NIRS negative with WT >0.5 mm), and NIRS-negative plaque-free wall sectors (>50% of the sector was NIRS negative with WT <0.5 mm). Consistently, the OCT-derived plaque classification was performed according to the following strategy: a sector was assigned to a specific category when at least 50% of that sector consisted of 1 OCT-derived vessel wall feature among fibrous cap atheroma, lipid-rich, fibrous, plaque-free wall. Since fibrous cap atheroma sectors were scarcely present (57/7101), no dedicated statistical analysis was performed, and the fibrous cap atheroma sectors were pooled together with the lipid-rich sectors. Hence, based on OCT imaging, all sectors were classified into 3 categories: lipid-rich, fibrous, and plaque-free wall. Finally, since calcium hampers PAV estimation, the presence of calcium was identified as bright signal with a lucent shadow, and all sectors containing IVUS-derived calcium (angle higher than 90° in the cross section) were excluded from the analysis.

A sector-based statistical analysis was conducted applying a linear mixed model where plaque progression (ΔPAV) was the dependent variable and WSS-based quantity classification, OCT, and NIRS plaque phenotypes were used as independent variables in terms of fixed factors.[9,24] The individual vessel was added to the model as a random factor. Random effects and correlations of sectors within individual vessels were accounted for by adopting unstructured covariance and correlation matrix in the linear mixed model. Statistical analysis for ΔPAV was adjusted for baseline PAV since plaques with different phenotypes might present with different baseline sizes. The Bonferroni correction was applied to adjust for multiple comparisons in the statistical analysis. Estimated mean value and standard error of the mean were presented.

The predictive potential of WSS-based quantities for plaque progression at the individual sector level was investigated in

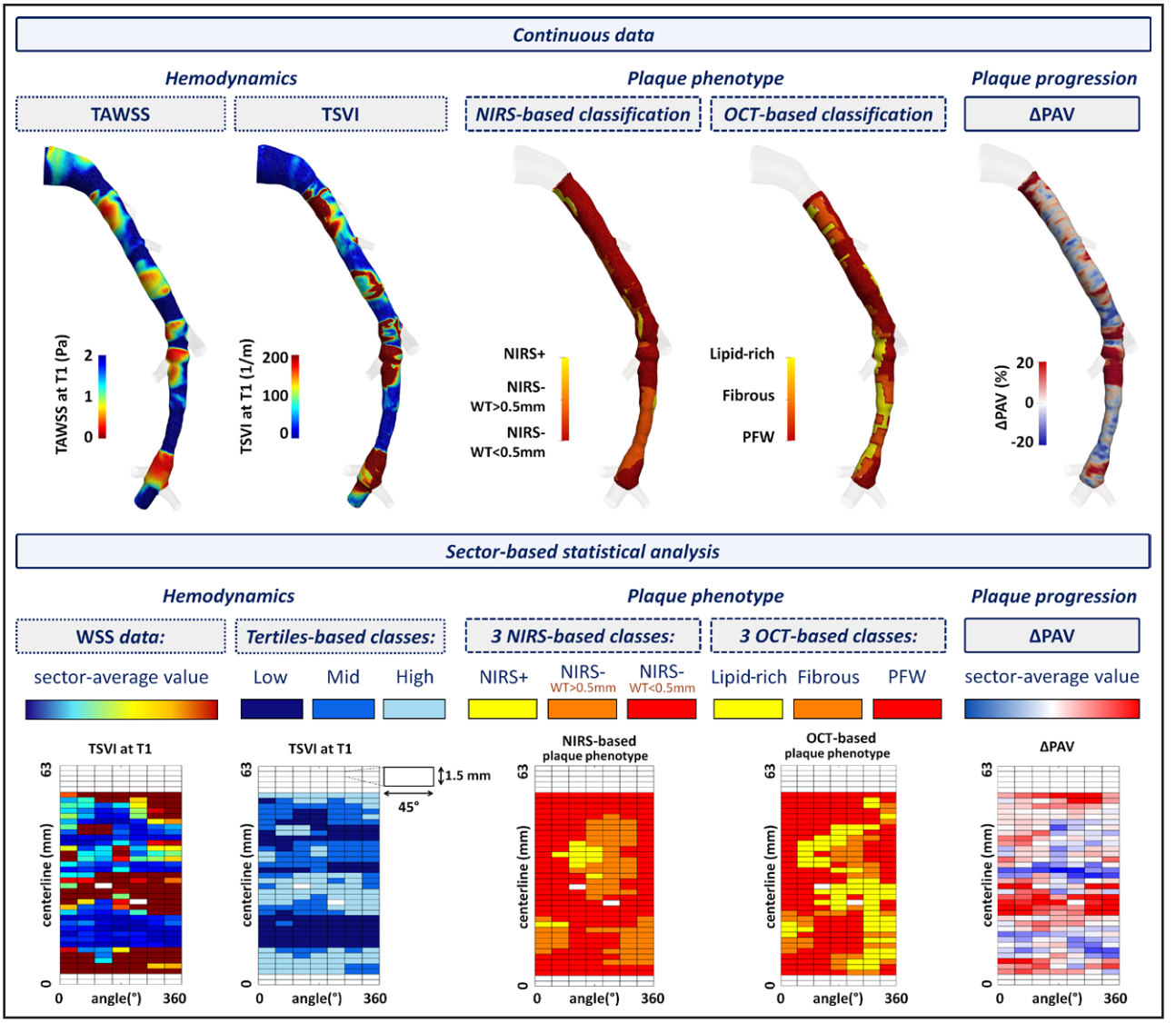

Figure 2. Methodology overview of sector-based statistical analysis.
Top, Explanatory examples of continuous maps of hemodynamics, plaque phenotype, and plaque progression quantities. **Bottom**, Sector-based maps of near-wall hemodynamics, plaque phenotype, and plaque progression quantities used for the statistical analysis. NIRS indicates near-infrared spectroscopy; OCT, optical coherence tomography; PAV, plaque atheroma volume; PFW, plaque-free wall; TAWSS, time-averaged wall shear stress; TSVI, topological shear variation index; WSS, wall shear stress; and WT, wall thickness.

terms of odds ratio, a measure of the influence of an event on a binary outcome (ie, manifestation or not of plaque progression). In detail, we classified as hemodynamically relevant the luminal surface sectors' exposure to low or high values of the WSS-based quantities based on vessel-specific tertiles. The combination of WSS-based quantities was also investigated. To determine the odds ratio, we classified as biologically relevant the luminal sectors exhibiting low (<33rd percentile) or high (>66th percentile) measured ΔPAV. Statistical significance was assumed for $P<0.05$.

RESULTS

The original IMPACT study data set consisted of 53 patients. Four patients withdrew consent at 1-month follow-up, 8 patients withdrew at 1 year from invasive imaging procedure. Four more of the remaining 41 patients were excluded because of insufficient image quality.[9] As a result, a complete data set was available on 37 patients (38 vessels). The patients' characteristics are reported in Table S2. Additionally, Table S3 reports the measured values of WT and PAV, together with their changes in T1 to T2 time interval.

The multidirectionality of the WSS as quantified by OSI and transWSS (Figure S2) was very low, with all OSI values lower than 0.04 (0.0007 [0.0003–0.003]) and transWSS values lower than 0.15 Pa (0.03 [0.02–0.06] Pa). Additionally, the observed very low OSI values made (by definition, see Table S1) RRT a replica of TAWSS. For these reasons, OSI, RRT, and transWSS were excluded from further analysis, considering the WSS signatures

captured by these quantities of second order in the herein analyzed data set of coronary arteries.

WSS Versus Plaque Progression

The distributions of ΔPAV, and baseline TAWSS and TSVI on the luminal surface of 9 explanatory cases (3 left anterior descending coronary artery, 3 left circumflex coronary artery, and 3 right coronary artery) are presented in Figure S3. Overall, a marked colocalization clearly emerged between plaque progression (high ΔPAV) and luminal surface areas exposed at baseline to low TAWSS and high TSVI.

These observations were confirmed by the results of sector-based statistical analysis (Figure 3; Table S4). In detail, vessel wall sectors exposed to high TSVI values at T1 exhibited significantly higher plaque progression (ΔPAV, 4.0% [95% CI, 2.6%–5.4%]) than sectors exposed to mid (2.2% [95% CI, 1.3%–3.2%]; P=0.002) or low (2.0% [95% CI, 0.9%–3.1%]; P=0.010) TSVI values. A clear even if not significant trend emerged also for the exposure to TAWSS, with the highest ΔPAV at plaque sectors experiencing low TAWSS at T1 (low, 3.6% [95% CI, 2.3%–4.8%]; mid, 2.4% [95% CI, 1.4%–3.4%]; high, 2.3% [95% CI, 1.0%–3.6%]).

Plaque Phenotypes and WSS Versus Plaque Progression

The observed link between WSS signatures and plaque progression emerged also for plaques with various phenotypes (Figure 4A and 4C). In detail, lipid-rich plaque sectors (NIRS+ and OCT lipid-rich) exposed to low TAWSS at T1 exhibited higher ΔPAV over the T2 to T1 time interval than lipid-rich sectors exposed to mid and high TAWSS (with statistical significance only for NIRS+, P=0.040 and P=0.008, respectively). Lipid-rich sectors exposed to high TSVI at T1 exhibited significantly higher plaque progression (ΔPAV) than sectors exposed to mid (P=0.007 for OCT; no significance for NIRS+) or low (P<0.001 for OCT; nearly significant for NIRS+, P=0.064) TSVI. Similar trends were observed for the other plaque phenotypes but with significantly lower plaque progression than the lipid-rich plaque sectors (Figure 4). Interestingly, the OCT-based fibrous plaque sectors did not differ in terms of plaque progression from the lipid-rich sectors, regardless of the exposure to low, mid, or high TAWSS or TSVI (Figure 4B and 4D).

Plaque phenotype acted synergistically with TAWSS or TSVI regarding plaque progression: at low TAWSS or high TSVI sectors in combination with lipid-rich plaque, ΔPAV values were higher than expected based on the individual contribution of hemodynamics (7.13±1.09% versus 3.80±0.66%, on average). Interestingly, if plaque phenotype was based on OCT, the synergism with TAWSS was less evident (Figure 4).

Individual data of Figure 4 are reported in Tables S5 and S6.

Effect of WSS-Based Quantity Combination on Plaque Progression

The analysis of the single/combined mechanical effect of TAWSS and TSVI on plaque progression is presented in terms of odds ratio (Figure 5A). A graphical sketch of the emerged significant predictions of ΔPAV levels by WSS signatures is also reported, together with the related percentage increase in the odds of the outcome (Figure 5B). In detail, each connecting link in Figure 5B represents an emerged significant prediction, while the reported percentage value is the percentage increase in the odds of plaque progression related to the exposure to a specific hemodynamic event at baseline (eg, an odds ratio of 1.37 corresponds to an increase in the odds of the outcome of 37%). Accuracy, positive, and negative predictive values related to plaque progression prediction tests are reported in Table S7.

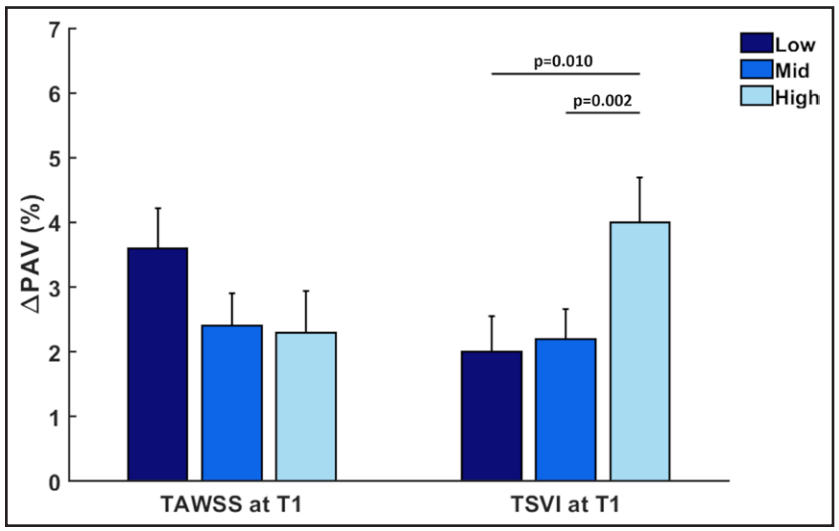

Figure 3. The link between plaque progression and hemodynamic variables.
Relationship between baseline (T1) time-averaged wall shear stress magnitude (TAWSS; **left**) and topological shear variation index (TSVI; **right**) levels and estimated plaque progression (expressed as plaque atheroma volume change [ΔPAV]). Estimated mean and SEM values are reported. The hemodynamic quantities were divided into low (dark blue bars), mid (blue bars), and high (light blue bars) tertiles per artery. Significant P values are also displayed. Individual data in the figure are reported in Table S4. Statistics: linear mixed-effects model.

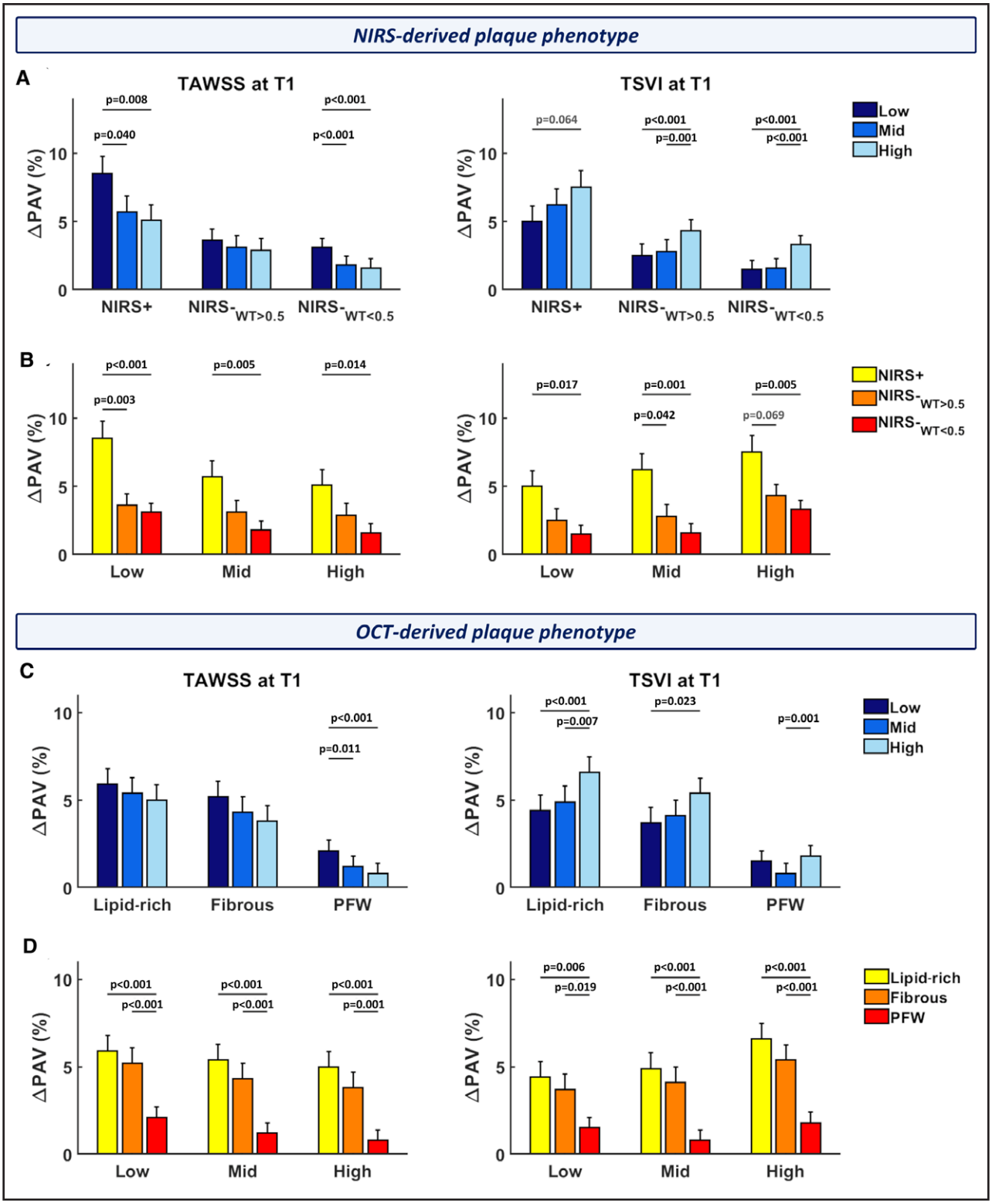

Figure 4. Link between plaque progression and hemodynamic variables for different plaque phenotypes. Relationship between baseline (T1) time-averaged wall shear stress magnitude (TAWSS; **left**) and topological shear variation index (TSVI; **right**) levels and estimated plaque progression (expressed as plaque atheroma volume change [ΔPAV]) for different near-infrared spectroscopy (NIRS; **top**)-derived and optical coherence tomography (OCT)-derived (**bottom**) plaque phenotypes. Estimated mean and SEM values are reported. The hemodynamic quantities were divided in low (dark blue bars), mid (blue bars), and high (light blue bars) tertiles per artery (**A** and **C**). NIRS-derived plaque phenotype groups were divided in NIRS+ (yellow bars), NIRS− with wall thickness (WT) >0.5 mm (orange bars), and NIRS− with WT <0.5 mm (red bars; **B**). OCT-derived plaque phenotype groups were divided into lipid-rich (yellow bars), fibrous (orange bars), and plaque-free wall (PFW; red bars; **D**). Significant and near-significance *P* values are displayed in black and gray, respectively. Individual data in the figure are reported in Tables S5 and S6. Statistics: linear mixed-effects model.

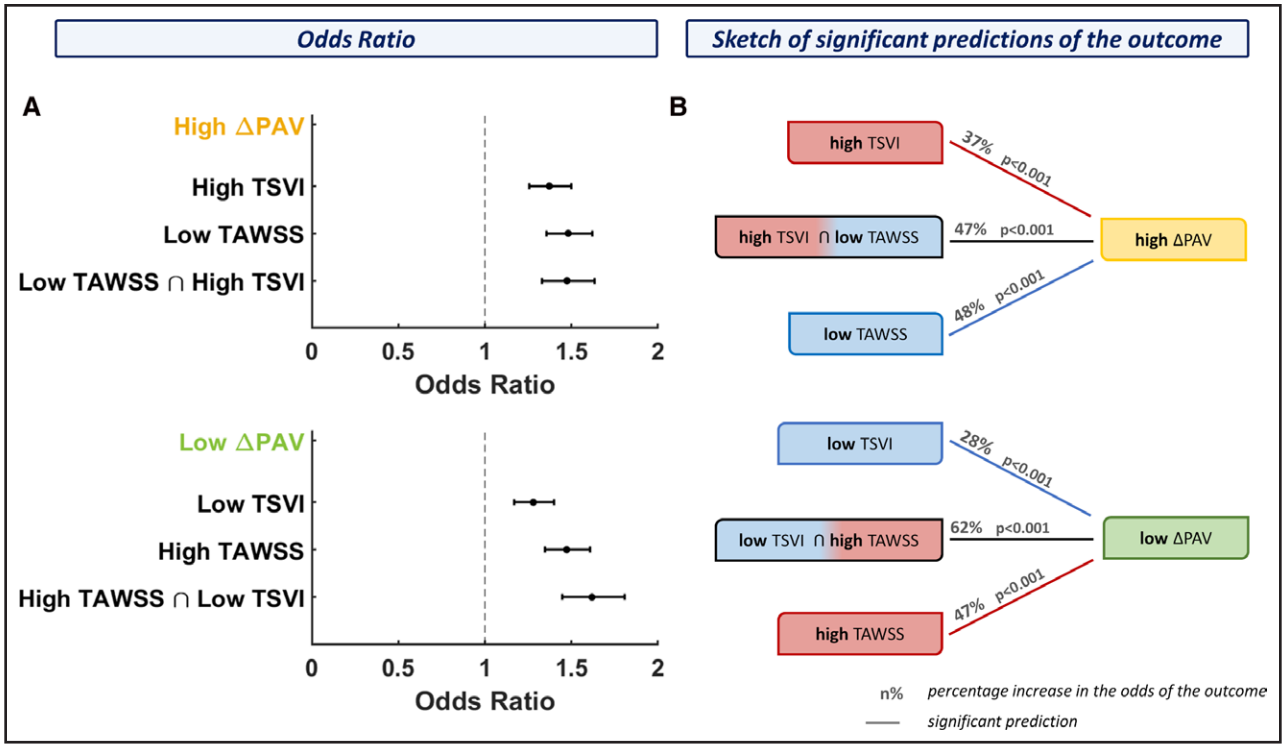

Figure 5. Predictive ability of hemodynamic variables for plaque progression.
A, Odds ratios with associated CI for hemodynamic events vs high (**top**) and low (**bottom**) plaque atheroma volume change (ΔPAV). **B**, Graphical sketch of the identified significant predictions of the biological event by the hemodynamic event, together with the associated percentage increase in the odds of the outcome. Each connecting link represents an emerged significant prediction, while the reported percentage value is the percentage increase in the odds of plaque progression related to the exposure to a specific hemodynamic event at baseline (eg, an odds ratio of 1.37 corresponds to an increase in the odds of the outcome of 37%). *P* value associated to each significant prediction is also reported. Red and blue colors are used to identify the high and low levels of the hemodynamic quantity, respectively. Statistics: Fisher exact test. TAWSS indicates time-averaged wall shear stress magnitude; and TSVI, topological shear variation index.

When considering the adverse outcome (ie, high ΔPAV), high TSVI at baseline was a good predictor of later high plaque progression (1.37 [1.25–1.50]; Figure 5). Comparable predictions of the adverse outcome emerged for the exposure to low TAWSS at baseline (1.48 [1.35–1.62]; Figure 5). However, the combination of high TSVI and low TAWSS did not improve plaque progression prediction capability (1.47 [1.33–1.63]).

Mirroring the analysis, the same approach was applied to the favorable outcome, that is, low ΔPAV (Figure 5). In detail, the exposure to low TSVI or high TAWSS showed comparable prediction of the favorable outcome (1.28 [1.17–1.40] and 1.47 [1.34–1.61], respectively), while their combination was an even stronger predictor of low ΔPAV (1.62 [1.44–1.80]) than low TSVI or high TAWSS solely.

DISCUSSION

This study integrated multimodal clinical imaging based on IVUS, NIRS, OCT, invasive Doppler flow measurements, and personalized CFD simulations to investigate (1) the dynamic changes in WSS signatures (in terms of TAWSS and TSVI) for predicting coronary artery plaque progression in humans and (2) the synergistic effect of TAWSS and TSVI and atherosclerotic plaque phenotypes on atherosclerotic plaque evolution.

We were able to conclude the following (Figures 3 and 4): (1) high variability in the contraction/expansion action exerted by WSS on the endothelium along the cardiac cycle (quantified by TSVI) is associated with plaque progression; (2) there is a clear (even if not significant) trend between baseline exposure to time-averaged WSS magnitude (quantified by TAWSS) and atherosclerotic plaque evolution, with low TAWSS characterizing vessels sectors where ΔPAV is high and vice versa; (3) high TSVI and low TAWSS at baseline, when combined with the lipid-rich plaque phenotype as determined by either NIRS or OCT, resulted in the highest plaque progression at 1-year follow-up; (4) in all the 3 NIRS- or OCT-derived plaque phenotype classes, the same trends characterized the association of atherosclerotic plaque progression with TSVI and TAWSS at T1, that is, where TSVI (TAWSS) is high (low), ΔPAV is high.

The present study represents the first prospective evaluation of the effect that the variability (along the cardiac cycle) of the WSS contraction/expansion action on coronary arteries endothelium, as

characterized by TSVI, has on atherosclerotic plaques progression in comparison to TAWSS, in hemodynamically stable patients. As recently suggested by animal studies,[13] the 2 WSS-based quantities capture different mechanical actions on the endothelial cells (Figure S1): the first, based only on the stress magnitude acting on the luminal surface (TAWSS); the second, based on the variations along the cardiac cycle in the thickening/rarefaction of the WSS field converging/diverging lines (TSVI). Although the luminal exposure to high TSVI may lead to similar biological end points as low TAWSS, these 2 WSS signatures quantify different stimuli transmitted to the endothelium, thus representing purportedly different processes from a mechanistic viewpoint.[13] Luminal exposure to low TAWSS might hamper endothelial cells' fusiform shaping in the main flow direction, inducing the relaxation of intracellular and cell-to-cell tension with the consequent widening of intercellular junctions, enhancing endothelial cells' proatherogenic susceptibility, and increasing of adhesion molecules expression and lipid infiltration in the wall.[3,4,14,15,35] Instead, high TSVI values at the endothelium indicate high spatial and temporal variability in the conformation of shear stress-induced tension state of the endothelial cells. Such a tension variability at the cell level, reflecting both on intracellular and intercellular mechanoreceptors, might (1) promote endothelium proinflammatory phenotype[16,35,36] and (2) cause an unstable cyclical shrinking/widening of cell-cell junction,[17,37] influencing endothelium permeability to atherogenic species.[3,17,18,36] This would favor biological mechanisms such as lipids wall infiltration that may, in turn, stimulate endothelial dysfunction,[5,38] thus potentially precipitating atherosclerosis progression.

The hypothesis of the 2 different WSS signatures differently stimulating the endothelium is supported by the analysis in Figure 6, reporting the extent of TSVI and TAWSS colocalization at the luminal sectors where high plaque progression was observed. It emerged that the colocalization of low TAWSS and high TSVI occurred in 24.0% of the high ΔPAV sectors, while only low TAWSS occurred in 38.8% of the sectors and only high TSVI in 38.7%, confirming that low TAWSS and high TSVI account for different hemodynamic stimuli, both promoting plaque progression. The extent of low TAWSS and high TSVI colocalization decreased to 19.7% when considering the entire data set.

The significant relationship between TSVI and markers of the atherosclerotic disease progression in human coronary arteries (1) confirms recent observations on the association of TSVI and vascular pathophysiology in other vascular beds or species[19–21] and (2) suggests that, in addition to low WSS,[4,7,9,39] also the high variability in the expansion and contraction action of the WSS on the endothelium may represent a relevant hemodynamic cue in coronary artery disease.

In this study, we also analyzed the impact of those 2 hemodynamics quantities on various plaque phenotypes. Our findings suggest that a biomechanical action quantified by high TSVI and by low TAWSS values on a lipid-rich plaque phenotype has an amplified effect on plaque progression, resulting in the highest values of ΔPAV at 1-year follow-up. In this regard, similar trends emerged between TSVI and ΔPAV and between TAWSS and ΔPAV for each class of plaque phenotype, but with TSVI showing more often statistically significant differences. These findings suggest a different role of the specific hemodynamic stimulus (low TAWSS or high TSVI) also in its synergistic action on plaque progression, when combined with plaque phenotypes.

As potential limitations of the study, in the numerical simulations, coronary walls were assumed to be rigid and the cardiac-induced motion was neglected, based on reported evidence that both wall elasticity and myocardial motion do not markedly affect the distribution of canonical WSS-based quantities.[40,41] We expect a similar result for TSVI. A small number of coronary artery models were used in the analysis (N=38). However, here, we

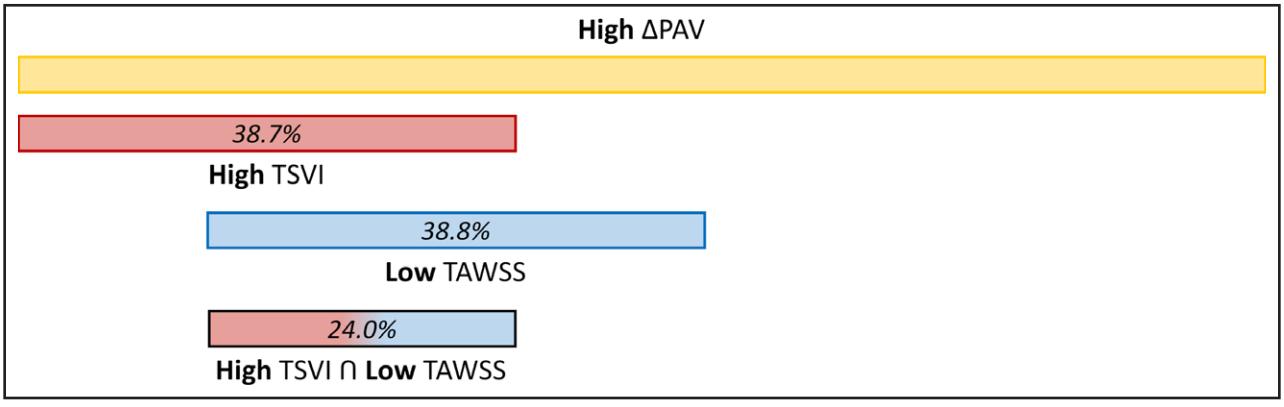

Figure 6. Graphical sketch of the colocalization of hemodynamic and biological events.
The percentage of high plaque progression sectors exposed to hemodynamically relevant events is reported. ΔPAV indicates plaque atheroma volume change; TAWSS, time-averaged wall shear stress magnitude; and TSVI, topological shear variation index.

considered multiple sectors within each coronary artery ($N_{sectors}$=9728), while statistically accounting for multiple measurements per vessel, and by doing so statistically significant relations emerged, revealing links between local hemodynamics, plaque phenotypes, and PAV. The classification of lipid-rich plaque was based on the percentage of each luminal sector (>50% was the adopted threshold) exhibiting an NIRS-positive signal, rather than on the plaque surface. Based on previous evidence,[24] we expect comparable results when focusing the analysis on luminal regions with the highest lipid content per 4-mm longitudinal segment.[42] Finally, the small number of patients and follow-up time did not allow for a direct association among hemodynamics, plaque phenotype, and clinical events and should be investigated in future studies.

The findings of this work contribute to pointing out the translational potential of CFD as a technology able to provide insights into vascular biology and to support decision-making in the treatment of CAD in daily clinical practice.[43,44] The current computer power and the increasingly realistic, personalized computer simulation of coronary hemodynamics enable to capture complex WSS signatures influencing coronary vascular pathogenesis,[21,43] highlighting regions at risk of plaque progression. Recent evidence demonstrating the feasibility of independent management by clinicians of CFD for CAD-related predictions,[21] combined with the profound interest recently expressed by interventional cardiologists in utilizing CFD simulations for the CAD management,[44] make the clinical translation of computational models a tangible near-future scenario.

In conclusion, the present study confirms the existence of links between the variability in WSS signatures (TSVI) and markers of atherosclerotic disease progression in coronary arteries, contributing to a more complete picture of the role of WSS in vascular pathophysiology. Overall, the findings from this work suggest that the quantified variability in the contraction/expansion action exerted by the WSS on the endothelium along the cardiac cycle (TSVI) is associated with plaque progression. Moreover, in case lipid-rich plaques are exposed to high TSVI, the highest plaque progression is observed. Therefore, the variability in the WSS action at the arterial luminal surface, in addition to low WSS, significantly contributes to a deeper understanding of the hemodynamic impact on the onset/development of coronary atherosclerosis.

ARTICLE INFORMATION

Received October 27, 2023; accepted January 26, 2024.

Affiliations

Polito^{BIO}Med Laboratory, Department of Mechanical and Aerospace Engineering, Politecnico di Torino, Turin, Italy (G.D.N., E.T., C.C., D.G., U.M.). Department of Cardiology, Biomedical Engineering, Erasmus MC, Rotterdam, the Netherlands (E.M.J.H., J.D., J.J.W.).

Sources of Funding

G. De Nisco, C. Chiastra, D. Gallo, and U. Morbiducci have been supported by the Italian Ministry of Education, University and Research (FISR2019_03221—CECOMES [CEntro di studi sperimentali e COmputazionali per la ModElliStica applicata alla chirurgia]). J.J. Wentzel has been supported by the European Research Council, Brussels, Belgium (grant number 310457).

Disclosures

None.

Supplemental Material

Tables S1–S7
Figures S1–S3
Video S1
Major Resources Table

REFERENCES

1. Mathers CD, Loncar D. Projections of global mortality and burden of disease from 2002 to 2030. *PLoS Med*. 2006;3:e442. doi: 10.1371/journal.pmed.0030442
2. Malek AM, Alper SL, Izumo S. Hemodynamic shear stress and its role in atherosclerosis. *JAMA*. 1999;282:2035–2042. doi: 10.1001/jama.282.21.2035
3. Chatzizisis YS, Coskun AU, Jonas M, Edelman ER, Feldman CL, Stone PH. Role of endothelial shear stress in the natural history of coronary atherosclerosis and vascular remodeling: molecular, cellular, and vascular behavior. *J Am Coll Cardiol*. 2007;49:2379–2393. doi: 10.1016/j.jacc.2007.02.059
4. Wentzel JJ, Chatzizisis YS, Gijsen FJH, Giannoglou GD, Feldman CL, Stone PH. Endothelial shear stress in the evolution of coronary atherosclerotic plaque and vascular remodelling: current understanding and remaining questions. *Cardiovasc Res*. 2012;96:234–243. doi: 10.1093/cvr/cvs217
5. Libby P, Ridker PM, Maseri A. Inflammation and atherosclerosis. *Circulation*. 2002;105:1135–1143. doi: 10.1161/hc0902.104353
6. Libby P, Hansson GK. From focal lipid storage to systemic inflammation: JACC review topic of the week. *J Am Coll Cardiol*. 2019;74:1594–1607. doi: 10.1016/j.jacc.2019.07.061
7. Stone PH, Saito S, Takahashi S, Makita Y, Nakamura S, Kawasaki T, Takahashi A, Katsuki T, Nakamura S, Namiki A, et al; PREDICTION Investigators. Prediction of progression of coronary artery disease and clinical outcomes using vascular profiling of endothelial shear stress and arterial plaque characteristics: the PREDICTION study. *Circulation*. 2012;126:172–181. doi: 10.1161/CIRCULATIONAHA.112.096438
8. Koskinas KC, Sukhova GK, Baker AB, Papafaklis MI, Chatzizisis YS, Coskun AU, Quillard T, Jonas M, Maynard C, Antoniadis AP, et al. Thin-capped atheromata with reduced collagen content in pigs develop in coronary arterial regions exposed to persistently low endothelial shear stress. *Arterioscler Thromb Vasc Biol*. 2013;33:1494–1504. doi: 10.1161/ATVBAHA.112.300827
9. Hartman EMJ, de Nisco G, Kok AM, Tomaniak M, Nous FMA, Korteland SA, Gijsen FJH, den Dekker WK, Diletti R, van Mieghem NMDA, et al. Wall shear stress–related plaque growth of lipid-rich plaques in human coronary arteries: an near-infrared spectroscopy and optical coherence tomography study. *Cardiovasc Res*. 2022;119:cvac178. doi: 10.1093/cvr/cvac178
10. Vergallo R, Papafaklis MI, Yonetsu T, Bourantas CV, Andreou I, Wang Z, Fujimoto JG, McNulty I, Lee H, Biasucci LM, et al. Endothelial shear stress and coronary plaque characteristics in humans: combined frequency-domain optical coherence tomography and computational fluid dynamics study. *Circ Cardiovasc Imaging*. 2014;7:905–911. doi: 10.1161/CIRCIMAGING.114.001932
11. Brown AJ, Teng Z, Evans PC, Gillard JH, Samady H, Bennett MR. Role of biomechanical forces in the natural history of coronary atherosclerosis. *Nat Rev Cardiol*. 2016;13:210–220. doi: 10.1038/nrcardio.2015.203
12. Peiffer V, Sherwin SJ, Weinberg PD. Does low and oscillatory wall shear stress correlate spatially with early atherosclerosis? A systematic review. *Cardiovasc Res*. 2013;99:242–250. doi: 10.1093/cvr/cvt044
13. Mazzi V, De Nisco G, Hoogendoorn A, Calò K, Chiastra C, Gallo D, Steinman DA, Wentzel JJ, Morbiducci U. Early atherosclerotic changes in coronary arteries are associated with endothelium shear stress contraction/expansion variability. *Ann Biomed Eng*. 2021;49:2606–2621. doi: 10.1007/s10439-021-02829-5
14. Davies PF. Flow-mediated endothelial mechanotransduction. *Physiol Rev*. 1995;75:519–560. doi: 10.1152/physrev.1995.75.3.519
15. Chiu JJ, Chien S. Effects of disturbed flow on vascular endothelium: pathophysiological basis and clinical perspectives. *Physiol Rev*. 2011;91:327–387. doi: 10.1152/physrev.00047.2009

16. Hur SS, del Álamo JC, Park JS, Li YS, Nguyen HA, Teng D, Wang KC, Flores L, Alonso-Latorre B, Lasheras JC, et al. Roles of cell confluency and fluid shear in 3-dimensional intracellular forces in endothelial cells. *Proc Natl Acad Sci USA*. 2012;109:11110–11115. doi: 10.1073/pnas.1207326109
17. Melchior B, Frangos JA. Shear-induced endothelial cell-cell junction inclination. *Am J Physiol Cell Physiol*. 2010;299:C621–C629. doi: 10.1152/ajpcell.00156.2010
18. Wang C, Baker BM, Chen CS, Schwartz MA. Endothelial cell sensing of flow direction. *Arterioscler Thromb Vasc Biol*. 2013;33:2130–2136. doi: 10.1161/ATVBAHA.113.301826
19. De Nisco G, Tasso P, Calò K, Mazzi V, Gallo D, Condemi F, Farzaneh S, Avril S, Morbiducci U. Deciphering ascending thoracic aortic aneurysm hemodynamics in relation to biomechanical properties. *Med Eng Phys*. 2020;82:119–129. doi: 10.1016/j.medengphy.2020.07.003
20. Morbiducci U, Mazzi V, Domanin M, De Nisco G, Vergara C, Steinman DA, Gallo D. Wall shear stress topological skeleton independently predicts long-term restenosis after carotid bifurcation endarterectomy. *Ann Biomed Eng*. 2020;48:2936–2949. doi: 10.1007/s10439-020-02607-9
21. Candreva A, Pagnoni M, Rizzini ML, Mizukami T, Gallinoro E, Mazzi V, Gallo D, Meier D, Shinke T, Aben JP, et al. Risk of myocardial infarction based on endothelial shear stress analysis using coronary angiography. *Atherosclerosis*. 2022;342:28–35. doi: 10.1016/j.atherosclerosis.2021.11.010
22. Tearney GJ, Regar E, Akasaka T, Adriaenssens T, Barlis P, Bezerra HG, Bouma B, Bruining N, Cho J, Chowdhary S, et al. Consensus standards for acquisition, measurement, and reporting of intravascular optical coherence tomography studies: a report from the International Working Group for Intravascular Optical Coherence Tomography Standardization and Validation. *J Am Coll Cardiol*. 2012;59:1058–1072. doi: 10.1016/j.jacc.2011.09.079
23. Hoogendoorn A, Kok AM, Hartman EMJ, de Nisco G, Casadonte L, Chiastra C, Coenen A, Korteland SA, van der Heiden K, Gijsen FJH, et al. Multidirectional wall shear stress promotes advanced coronary plaque development: comparing five shear stress metrics. *Cardiovasc Res*. 2020;116:1136–1146. doi: 10.1093/cvr/cvz212
24. Hartman EMJ, De Nisco G, Kok AM, Hoogendoorn A, Coenen A, Mastik F, Korteland SA, Nieman K, Gijsen FJH, van der Steen AFW, et al. Lipid-rich plaques detected by near-infrared spectroscopy are more frequently exposed to high shear stress. *J Cardiovasc Transl Res*. 2021;14:416–425. doi: 10.1007/s12265-020-10072-x
25. van der Giessen AG, Schaap M, Gijsen FJH, Groen HC, van Walsum T, Mollet NR, Dijkstra J, van de Vosse FN, Niessen WJ, de Feyter PJ, et al. 3D fusion of intravascular ultrasound and coronary computed tomography for in-vivo wall shear stress analysis: a feasibility study. *Int J Cardiovasc Imaging*. 2010;26:781–796. doi: 10.1007/s10554-009-9546-y
26. De Nisco G, Kok AM, Chiastra C, Gallo D, Hoogendoorn A, Migliavacca F, Wentzel JJ, Morbiducci U. The atheroprotective nature of helical flow in coronary arteries. *Ann Biomed Eng*. 2019;47:425–438. doi: 10.1007/s10439-018-02169-x
27. De Nisco G, Hoogendoorn A, Chiastra C, Gallo D, Kok AM, Morbiducci U, Wentzel JJ. The impact of helical flow on coronary atherosclerotic plaque development. *Atherosclerosis*. 2020;300:39–46. doi: 10.1016/j.atherosclerosis.2020.01.027
28. De Nisco G, Chiastra C, Hartman EMJ, Hoogendoorn A, Daemen J, Calò K, Gallo D, Morbiducci U, Wentzel JJ. Comparison of swine and human computational hemodynamics models for the study of coronary atherosclerosis. *Front Bioeng Biotechnol*. 2021;9:731924. doi: 10.3389/fbioe.2021.731924
29. Chiastra C, Gallo D, Tasso P, Iannaccone F, Migliavacca F, Wentzel JJ, Morbiducci U. Healthy and diseased coronary bifurcation geometries influence near-wall and intravascular flow: a computational exploration of the hemodynamic risk. *J Biomech*. 2017;58:79–88. doi: 10.1016/j.jbiomech.2017.04.016
30. Ponzini R, Vergara C, Redaelli A, Veneziani A. Reliable CFD-based estimation of flow rate in haemodynamics measures. *Ultrasound Med Biol*. 2006;32:1545–1555. doi: 10.1016/j.ultrasmedbio.2006.05.022
31. van der Giessen AG, Groen HC, Doriot PA, de Feyter PJ, van der Steen AFW, van de Vosse FN, Wentzel JJ, Gijsen FJH. The influence of boundary conditions on wall shear stress distribution in patients specific coronary trees. *J Biomech*. 2011;44:1089–1095. doi: 10.1016/j.jbiomech.2011.01.036
32. Ku DN, Giddens DP, Zarins CK, Glagov S. Pulsatile flow and atherosclerosis in the human carotid bifurcation. Positive correlation between plaque location and low oscillating shear stress. *Arteriosclerosis*. 1985;5:293–302. doi: 10.1161/01.atv.5.3.293
33. Himburg HA, Grzybowski DM, Hazel AL, LaMack JA, Li XM, Friedman MH. Spatial comparison between wall shear stress measures and porcine arterial endothelial permeability. *Am J Physiol Heart Circ Physiol*. 2004;286:H1916–H1922. doi: 10.1152/ajpheart.00897.2003
34. Peiffer V, Sherwin SJ, Weinberg PD. Computation in the rabbit aorta of a new metric - the transverse wall shear stress - to quantify the multidirectional character of disturbed blood flow. *J Biomech*. 2013;46:2651–2658. doi: 10.1016/j.jbiomech.2013.08.003
35. Hahn C, Schwartz MA. Mechanotransduction in vascular physiology and atherogenesis. *Nat Rev Mol Cell Biol*. 2009;10:53–62. doi: 10.1038/nrm2596
36. Naruse K, Sokabe M. Involvement of stretch-activated ion channels in Ca2+ mobilization to mechanical stretch in endothelial cells. *Am J Physiol*. 1993;264:C1037–C1044. doi: 10.1152/ajpcell.1993.264.4.C1037
37. Lei M, Kleinstreuer C, Truskey GA. A focal stress gradient-dependent mass transfer mechanism for atherogenesis in branching arteries. *Med Eng Phys*. 1996;18:326–332. doi: 10.1016/1350-4533(95)00045-3
38. Choi BJ, Prasad A, Gulati R, Best PJ, Lennon RJ, Barsness GW, Lerman LO, Lerman A. Coronary endothelial dysfunction in patients with early coronary artery disease is associated with the increase in intravascular lipid core plaque. *Eur Heart J*. 2013;34:2047–2054. doi: 10.1093/eurheartj/eht132
39. Samady H, Eshtehardi P, McDaniel MC, Suo J, Dhawan SS, Maynard C, Timmins LH, Quyyumi AA, Giddens DP. Coronary artery wall shear stress is associated with progression and transformation of atherosclerotic plaque and arterial remodeling in patients with coronary artery disease. *Circulation*. 2011;124:779–788. doi: 10.1161/CIRCULATIONAHA.111.021824
40. Zeng D, Ding Z, Friedman MH, Ethier CR. Effects of cardiac motion on right coronary artery hemodynamics. *Ann Biomed Eng*. 2003;31:420–429. doi: 10.1114/1.1560631
41. Eslami P, Tran J, Jin Z, Karady J, Sotoodeh R, Lu MT, Hoffmann U, Marsden A. Effect of wall elasticity on hemodynamics and wall shear stress in patient-specific simulations in the coronary arteries. *J Biomech Eng*. 2020;142:245031–2450310. doi: 10.1115/1.4043722
42. Goldstein JA, Madden SP, Sum ST, Dixon SR, Madder RD, Muller JE. Assessment of plaque composition with near-infrared spectroscopy. *Curr Cardiovasc Imaging Rep*. 2011;4:298–308. doi: 10.1007/s12410-011-9095-3
43. Candreva A, De Nisco G, Lodi Rizzini M, D'Ascenzo F, De Ferrari GM, Gallo D, Morbiducci U, Chiastra C. Current and future applications of computational fluid dynamics in coronary artery disease. *Rev Cardiovasc Med*. 2022;23:377. doi: 10.31083/j.rcm2311377
44. Chiastra C, Zuin M, Rigatelli G, D'Ascenzo F, De Ferrari GM, Collet C, Chatzizisis YS, Gallo D, Morbiducci U. Computational fluid dynamics as supporting technology for coronary artery disease diagnosis and treatment: an international survey. *Front Cardiovasc Med*. 2023;10:1216796. doi: 10.3389/fcvm.2023.1216796